Effect of chemical bonding on positive secondary-ion yields in sputtering

K. Mann and M. L. Yu
IBM Thomas J. Watson Research Center, Yorktown Heights, New York 10598
(Received 4 November 1986)

We have studied the effect of chemical bonding on the emission of positive secondary ions from solid surfaces in static mode sputtering. In all the three systems investigated, N-Si(100), O-Si(100), and O-Ge(111), the Si^+ and Ge^+ yields were enhanced by at least 2 orders of magnitude. X-ray photoemission showed that the ion yields were linearly related to the amount of surface nitrides or oxides formed during the reactions. The ion yields were site specific and showed emission-velocity and angle dependences. The results are compared to the predictions of a recently proposed bond-breaking model.

I. INTRODUCTION

When an energetic primary ion impinges on a solid, the momentum transfer can cause the sputtering of surface atoms from the surface, and a certain fraction of these ejected atoms are ionized. The formation of these *secondary ions* constitutes the basis of secondary-ion mass spectrometry (SIMS).[1] The prevailing view of the ionization process is that the sputtered atoms exchange electrons diabatically with the solid surface.[2] An electron tunneling model[3] has been developed for the ionization of atoms sputtered from metallic targets. This theory has been successfully applied to explain the emission of both positive- and negative-secondary-ion emission in certain systems.[3–5] Recently[6] we have presented evidence for another category of secondary-ion production where the charge fraction depends more on the local chemical bonding, than the global electronic state of the surface. We proposed that ionization can result from the rapid breaking of the local bond. In this paper, we shall present in more detail the experimental evidence that led to these conclusions.

The idea of ionization by bond breaking started with the observation that the ion fraction is very sensitive to surface chemistry.[7,8] The positive-metal-ion yield from an oxygen or other electronegative element covered metal surface can easily exceed the *intrinsic* ion yield from a clean metal surface, under similar sputtering conditions with an inert primary ion beam, by three orders of magnitude.[8] Since oxidation usually changes the sputtering rate only by factors of 2 or so, the phenomenon is mainly caused by a chemical enhancement of the ionization probability. In a recent experiment,[9] where both the sputtered neutral and ionized atoms were measured, the ionization probability of sputtered silicon atoms from an oxidized silicon surface was found to reach as high as 0.3. In fact, it is a regular practice in SIMS analysis to use oxygen primary-ion beams for sputtering to enhance the detection sensitivity.

If the interaction is indeed very local, phenomenologically the secondary-ion yield I_M^+ of element M would be the sum of the contributions from different bonding configurations (i) involving M:

$$I_M^+ = \sum_i f_i P_i^+ Y_i i_p \ , \tag{1}$$

where f_i, P_i^+, and Y_i are the concentration, ionization probability, and partial sputtering coefficient of the M atoms bonded in the ith configuration, and i_p is the primary-ion beam current. In the first approximation, all the P's and Y's are constants specific to the chemical configuration and are independent of the concentration. The linearity between I_A^+ and f_i is the unique feature of this localized interaction picture which however, has not been explicitly verified. Equation (1) is difficult to apply since the usual experimental observable is c_0, the concentration of the electronegative species (e.g., oxygen), and not f_i. A frequently measured quantity is the ionization probability $\tilde{P}^+$ defined as the ratio of the secondary-ion yield I_M^+ to the sputtering yield $\tilde{Y}$ as determined by erosion experiments. The latter is actually an averaged value given by the following:

$$\tilde{Y} = \sum_i f_i Y_i i_p \ . \tag{2}$$

The relation between c_0 and f_i depends very much on the surface reaction kinetics in the individual experiment. Both I_M^+ and Y have in general nonlinear dependences on the concentration of the electronegative species, and these relations are hard to predict. Hence the validity of Eq. (1) is not obvious, and the ion yield is rarely found to be linear with c_0. For example, the reported oxygen coverage dependences of the sputtering of Si^+ from silicon surfaces ranges from linear at very low coverages (<3 at. %) (Ref. 10) to power-law dependences,[10–12] to exponential dependences[13] when oxygen was introduced under ion bombardment conditions. In our experiment we have selected model chemical systems and specific reaction conditions to simplify the relation between f_i and c_0, which was monitored by x-ray photoemission (XPS). We have succeeded to observe the validity of Eq. (1) for Si^+ sputtered from oxidized and nitridized Si(100) surfaces, and for Ge^+ sputtered from oxidized Ge(111) surfaces.

II. EXPERIMENTAL PROCEDURE

The experiment was performed in an ultrahigh-vacuum system consisting of an analytical chamber and a preparation chamber. The turbo-pumped preparation chamber has a base pressure of 2×10^{-10} Torr and is equipped with a Varian low-energy electron diffraction (LEED) apparatus, a sputter ion gun for sample cleaning, and a dosing tube for gas introduction. The analytical chamber which is connected to the preparation chamber through a gate valve has a base pressure less than 1×10^{-10} Torr and is equipped with a Leybold EA-11 hemispherical energy analyzer, a Mg $K\alpha$ x-ray source for XPS, and a He lamp for ultraviolet photoemission (UPS). The sputtering experiment was performed with *in situ* XPS to monitor the coverage and the chemical state of the surface. The surface reactions (e.g., oxidation, nitridation) were induced thermally and sputtering was kept to a minimum (static mode[8]) to reduce ion-beam-induced chemistry and radiation damage to a negligible level. The coverage of the electronegative species was kept close to the monolayer range so that the information from both SIMS and XPS originate from the same reacted layer.

The Si(100) and Ge(111) samples were cut from 10 Ω cm n-type Si wafers which had 7000 Å of Ta film deposited on the back side for electrical conductivity. They were mounted by small Ta clamps on the sample holder and direct current heating was used. The sample temperature was monitored by an infrared pyrometer and the emissivity correction was determined by calibrating against an optical pyrometer from 650—900 °C.

After mounting into vacuum, the Si(100) samples were cleaned either by Ar^+ sputtering (1 μA/500 eV, 1—2 h) or, alternatively, following a three-step heating procedure (10 h at 600 °C, 5 min at 900 °C, 20 s at 1050 °C). Both treatments yielded a carbon- and oxide-free Si surface as monitored by XPS. LEED showed a sharp $p(2\times1)$ reconstruction pattern, whereas the UPS (He I) spectra exhibited the characteristic surface-state peak near the valence-band edge. The Ge(111) samples were simply cleaned by heating at 650 °C, leading to a sharp and intense surface state near the valence-band edge in UPS and the (2×8) overstructure in LEED.

In the sputtering experiment, the sample surfaces were bombarded with an Ar^+ beam (1 nA/500 eV, incident at $\simeq$30° off normal), which was rastered over a surface area of 4×4 mm^2 in order to provide for proper static mode SIMS conditions. Secondary ions (positive or negative) with different emission energies were first selected by an electrostatic energy filter of about 0.5-eV resolution without the use of an extraction field[14] and afterwards detected with a quadrupole mass spectrometer. Geometrically the entrance aperture of the energy filter subtended a cone of about 17° semiapex angle at the bombardment spot. Hence a qualitative comparison of sputtered ion yields at different emission angles could be made by changing the tilt of the sample. But since the angle between the primary-ion beam and the axis of the detector was fixed at 64.3°, rotating the sample caused changes both in the angle of incidence of the Ar^+ beam and the angle of detection.

Starting from the clean surface, oxygen or nitrogen was cumulatively absorbed on the samples, and the secondary-ion yields were measured as a function of the oxygen (nitrogen) coverage which was monitored by measuring the area under the XPS O 1s or N 1s peak. Simultaneously, we examined the adsorbate-induced chemical shifts of the substrate core-level peaks Si 2p and Ge 3d in order to study the oxide (nitride) growth. The surface sensitivity of XPS was enhanced by using a grazing emission angle (80° with respect to the surface normal). XPS and SIMS sampling depths were then of the same order ($\simeq$3 Å).

III. RESULTS

A. N-Si(100)

The first model system we studied is the effect of nitridation on the sputtering of Si^+ from Si(100) surfaces. Nitrogen was cumulatively adsorbed on Si(100) at high temperature (1000 °C). Owing to the low reaction rate, high exposures up to 6×10^6 L (1L=1 langmuir=10^{-6} Torr sec) at 10^{-3} Torr had to be used to reach a monolayer coverage. In accordance with observations by Schrott *et al.*,[15] nitrogen did not produce any extra LEED patterns at this temperature. The $p(2\times1)$ overstructure vanished gradually, accompanied by an increase in background intensity.

The nitridation process was monitored by the binding energy of the Si 2p core level. Starting from a clean Si(100) surface, the nitridation process lead to a shoulder and finally to a broad second peak at higher binding energy, the intensity of which increased with increasing exposure. The center of gravity of the shifted peak did not change its position for the different N_2 exposures, or in other words, the relative distribution of the various nitrides remained constant. The amount of this chemical shift was found to be 3.15 ± 0.15 eV, which we attribute to the formation of Si_3N_4 as the predominant species in the submonolayer nitridation process.[16] Hence we can assume with confidence that the amount of Si_3N_4 formed is directly proportional to the nitrogen coverage. With UPS we observed a depletion of the surface states upon nitridation. At the highest N_2 exposure (monolayer) the midpoint of the valence band edge was about 2.9 eV from the Fermi level. For comparison, the bulk Si_3N_4 band gap is about 5.0 eV (Ref. 17).

The sputtered Si^+ yield during the static mode Ar^+ bombardment of the clean Si(100) surface was barely above the noise level. Nitridation of the silicon surface up to a monolayer (1 ML$\simeq7\times10^{14}$ cm^{-2}) enhanced the Si^+ yield by at least 150 times as shown by the semilog plot of Si^+ yield versus nitrogen coverage, in Fig. 1(a). The most direct indication of a localized interaction for Si^+ formation is shown in Fig. 1(b), where the Si^+ yields with emission energies 8 and 17 eV and fixed emission angle $\theta=45°$ are plotted against the nitrogen coverage in a linear scale. Except for the case of very small exposures (<0.04 ML), we found a strong linear increase of the Si^+ yield with increasing nitrogen coverage, indicating that the Si^+ emission is directly proportional to the number of Si_3N_4 mole-

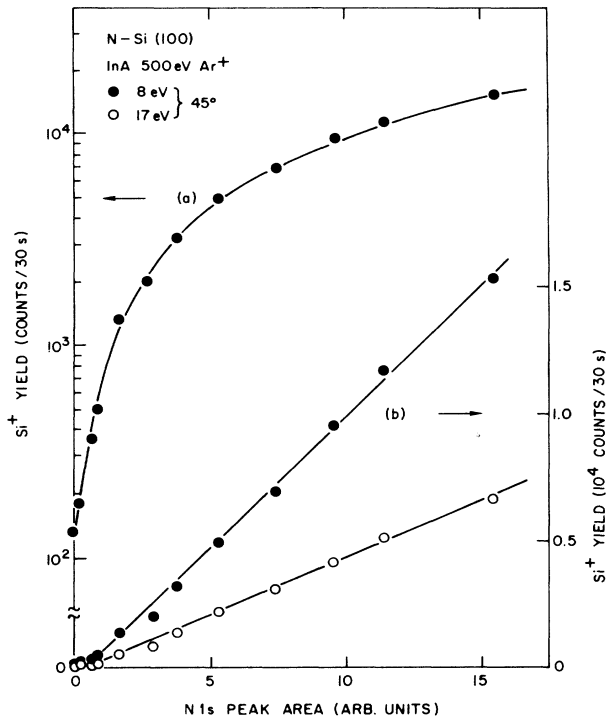

FIG. 1. Sputtered Si^+ yield as a function of nitrogen coverage for two different emission energies 8 and 17 eV and emission angle $\theta=45°$. The maximum coverage was estimated to be about 7×10^{14} cm^{-2}. Curve (a) shows that nitridation enhanced the Si^+ yield by practically 2 orders of magnitude.

cules formed during the nitridation process. The deviation observed at very low coverage is probably because low nitrogen concentration favors the formation of intermediate nitrides. However the quantity was too small to be identified by our XPS measurements. According to Eq. (1),

$$I_{Si}^{+}=(f_0P_0^{+}Y_0+f_1P_1^{+}Y_1)i_p\ . \tag{3}$$

The subscripts 0 and 1 represent unreacted Si and Si_3N_4, respectively. Since the Si^+ yield from a clean Si surface ($f_0=1$, $f_1=0$) is over 150 times less than that from a fully nitrided surface ($f_0=0$, $f_1=1$), we conclude that $P_0^{+}Y_0 \ll P_1^{+}Y_1$, and $I_{Si}^{+}\simeq f_1P_1^{+}Y_1i_p$ where f_1 is proportional to the nitrogen coverage. Hence, to a good approximation, our data is consistent with Eq. (1).

A similar linear behavior as in Fig. 1(b) was also found at other emission angles. Since we cannot distinguish the angular dependence of sputtering yield from that of the ionization probability, detailed angular measurements were not pursued.

For the highest exposure of Fig. 1, we measured the distribution of the sputtered positive molecular ions. A rather strong signal was found at mass 70 ($I_{70}/I_{28}\simeq0.25$) indicating that Si_2N^+ is the most abundant ionic molecular species formed during the sputtering event. Si_2N was also observed in the thermal desorption experiments reported by Schrott *et al.*[15]

B. O-Si(100)

Similar to the case of nitrogen, the adsorption of oxygen on silicon surfaces can enhance the sputtering of Si^+ by over 2 orders of magnitude. We have reported preliminary observations showing a linear relation between the Si^+ yield with the oxygen coverage for room-temperature adsorption.[2,18] However, we found that the result was not always reproducible. The growth process of suboxides on the silicon surface apparently depends on the sample history and the exact dosing procedure. Oxidation at 600 °C eliminated this problem. Oxidation caused a diffused background in the LEED pattern suggesting that there was no long-range order in the oxides formed.

For oxygen adsorption on Si(100) at 600 °C, we found *two regions* of oxygen coverages, both exhibiting a linear increase of the Si^+ yield with oxygen coverage (Fig. 2). The transition occurred at a coverage of about 7×10^{14} cm^{-2}, i.e., very close to a monolayer. The chemical shift of the Si $2p$ peak indicates that a mixture of suboxides was formed in the low coverage region (<1 ML), similar to that reported by Hollinger and Himpsel.[19] This is shown by the broadening of the higher binding-energy side of the Si $2p$ peak (Fig. 3, curves b and c). According to Ref. 19, this mixture is consisted of silicon atoms bonded to one, two, three, and four oxygen atoms with decreasing concentration. The difference spectra (Fig. 3, b-a and c-a) with respect to the clean silicon surface indicate that the relative distribution of the various oxides remained constant within our experimental accuracy, even though our XPS measurements did not have enough energy resolution to separate the various components. This implies that the amount of suboxides formed was simply proportional to the oxygen coverage. With further thermal oxidation (the second linear region in Fig. 2), the amount of suboxides (SiO_x) formed stayed practically constant, but the Si $2p$ peak showed an increase in the formation of SiO_2 where every silicon atom bonds to four oxygen

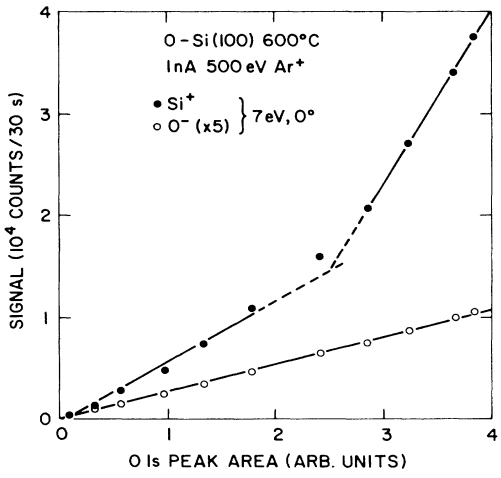

FIG. 2. Sputtered Si^+ and O^- yields from oxygenated Si(100) surface at different oxygen coverages. The maximum coverage was estimated to be less than two monolayers.

atoms. This is evident from the broad peak at -102.5 eV on curve d while the difference spectrum (d-c) shows the SiO_2 peak at -103.0 eV. By decomposing the XPS Si $2p$ spectra, we determined the amount of silicon atoms in the form of suboxide f_{SiO_x} and SiO_2 f_{SiO_2}. Both are linear with the oxygen coverage.

According to Eq. (1), the Si^+ yield can be written as:

$$I_{Si}^+ = (f_0 P_0^+ Y_0 + f_1 P_1^+ Y_1 + f_2 P_2^+ Y_2 - \alpha f_2 f_{1(\max)} P_1^+ Y_1) i_p \ , \quad (4)$$

Here subscripts 0, 1, and 2 represent unreacted Si, silicon suboxide, and SiO_2 respectively. α is a shielding factor which accounts for the possible shielding of the SiO_x molecules from contributing to the secondary ion yield, by the SiO_2 molecules grown in the second stage which may be lying on top. The net result is to have an effective $P_2^+ Y_2$ equal to $P_2^+ Y_2 - \alpha f_{1(\max)} P_1^+ Y_1$ as the coefficient for f_2. Since α was not experimentally accessible, we shall use the effective value. Similar to the N-Si case, the ion yield from the unoxidized area is very small and can be neglected. Hence the Si^+ yield can be decomposed into two components, and each increases linearly with f_{SiO_x} and f_{SiO_2}, respectively as shown by Fig. 4. Ideally, the slopes in Fig. 4 should give us the values of P^+Y. But without knowing the transmission of the mass spectrometer, we can only determine the yield ratio $Y_R \equiv (P_2^+ Y_2 / P_1^+ Y_1)$. Figure 4 shows that the yield ratio depends also on the emission energy. Y_R was found to be 3.5, 2.7, and 2.6 for Si^+ emitted with 8, 16, and 21 eV, respectively. However, we found that the yield ratio is independent of the emission angle. In this experiment we had no means to determine separately P^+ and Y. There is no known way to determine Y in the static mode unless the neutral fraction is also being measured.

The next most abundant secondary ion was O^- whose yield was about 1 order of magnitude smaller than that of Si^+ (Fig. 2). The O^- yield was found to be directly proportional to the oxygen coverage over the whole range, indicating that the chemical state of the oxygen atoms did not change much in the two regions. The molecular ions SiO^+ and Si_2^+ were another factors of 2 and 3 smaller. Similar to Si^+, they both showed linear dependences on the oxygen coverages but with different slopes at both the coverage regions. The SiO^+ yield increased rapidly in the SiO_2 region, but the Si_2^+ yield was practically unchanged suggesting a correlation to the lack of Si-Si neighbors in SiO_2.

C. O-Ge(111)

We also examined the effect of oxidation on the emission of Ge^+ from a Ge(111) surface. The experimental conditions were identical to those used for the O-Si(100) system. O_2 was cummulatively adsorbed at 270 °C. At this temperature the result was reproducible and the sticking coefficient is about 1 order of magnitude larger than

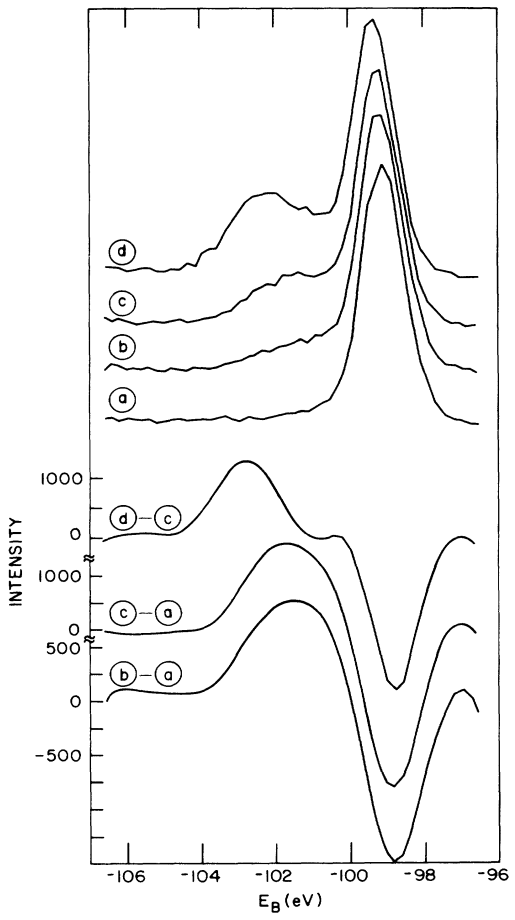

FIG. 3. Curves (a)—(d) show the XPS Si $2p$ spectra at various stages of oxidation of Si(100) at 600 °C: (a) clean, (b) 6L, (c) 14 L, (d) 1200 L. The lower three curves are difference spectra.

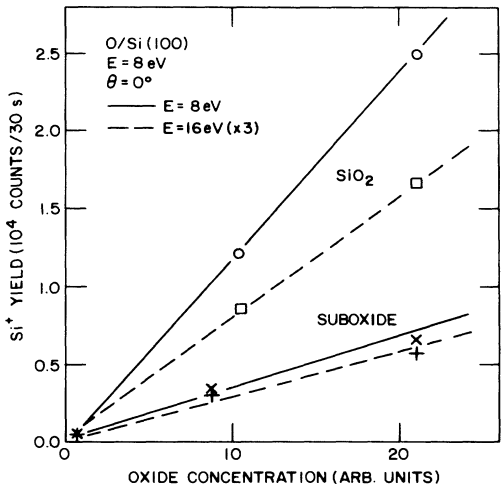

FIG. 4. Sputtered Si^+ yield as a function of the concentration of silicon suboxides and dioxide formed for two emission energies 8 and 16 eV.

that at room temperature. However, it still required about 10^6 L of exposure to reach saturation. The Ge^+ secondary ion yield from a clean Ge(111) surface was barely detectable (few counts per second). Oxidation of the Ge(111) surface also increased the Ge^+ yield from this intrinsic value by over 2 orders of magnitude. Figure 5 shows a linear plot of the Ge^+ yields as a function of the oxygen coverage, as represented by the area under the XPS O 1s peak, for 7- and 14-eV emission energies. Similar to the O-Si(100) results, we observed two different regions of the oxygen coverage, both exhibiting a linear increase of Si^+ yield, but with totally different slopes. The maximum oxygen coverage was about two monolayers.

The reason for the observation of two linear sections with different slopes is similar to the O-Si(100) case. Two oxide phases were formed in succession. We used the XPS Ge 3d peak to monitor the various stages of oxygen adsorption. Starting from the clean Ge(111) surface, we observed the growth of a broad suboxide peak which was shifted by $\simeq$1.9 eV to higher binding energies, and which finally reached about half the intensity of the elemental peak. The difference spectra indicate that the amount of suboxide formed is proportional to the oxygen coverage. The LEED (2×8) pattern of the clean Ge(111) surface slowly faded away upon oxygen adsorption, without the appearance of any extra spots. At about the coverage where the first linear section of Fig. 5 ends, the (2×8) reconstruction pattern completely vanished, whereas the weak (1×1) spots from the bulk structure were still visible. Further oxidation did not affect the suboxide peak height anymore but lead to a gradual shift of the Ge 3d peak to even higher energies (2.4 eV). We identify this second adsorption phase as the growth of GeO_2 (Ref. 20). It was again linear with the increase in oxygen coverage. This second oxidation stage started at about the same oxygen exposure where the high-coverage linear part of the Ge^+ yield began ($\simeq$1 monolayer). Therefore, the linear sections of Fig. 5 are directly related to these two different oxidation phases. At very low oxygen coverages, there was some deviation from linearity. We suspect that another form of suboxide was present. Unfortunately, our XPS was not sensitive enough to identify it.

By decomposing the XPS Ge 3d spectra, we measured the amount of germanium suboxide and dioxide formed as expressed by their Ge content. Using the same argument as in the O-Si case, the Ge^+ yield can be written in the form of Eq. (1):

$$I^+_{Ge}=(f_0P_0^+Y_0+f_1P_1^+Y_1+f_2P_2^+Y_2)i_p \ . \quad (5)$$

Here the subscripts 0, 1, and 2 denote unreacted germanium, germanium suboxide, and dioxide respectively. The contribution from the unreacted germanium is however negligible. Figure 6 shows directly that the increment in Ge^+ yield is indeed linear with the increase of suboxide or dioxide concentration in the two regions. GeO_2 with the higher oxygen coordination number is more efficient in promoting the emission of Ge^+. The yield ratio $Y_R \equiv (P_2^+Y_2)/(P_1^+Y_1)$ is about 6.5 for Ge^+ emitted normal to the surface and with 7-eV kinetic energy.

This sensitivity to chemical bonding is energy and strongly angular dependent. To demonstrate the phenomenon, all data in Fig. 7 have been normalized to the (7 eV/0°) results at the end of the first linear section (22 O 1s units). Upon further oxidation, the Ge^+ signal increases much more rapidly at large emission angles θ, whereas the energy dependence is comparatively weak (7 eV/30° versus 36 eV/30°). Similar to the O-Si(100) result, the sensitivity to the bonding configuration is larger for smaller emission energies.

In spite of the strong angular dependence there is a complete lack of correlation with the normal component of the emission velocity $v_z=(2E/m)^{1/2}\cos\theta$. As shown in Fig. 7, the slope increase for (7 eV/0°) and (36 eV/64°) is totally different, although these spectrometer settings

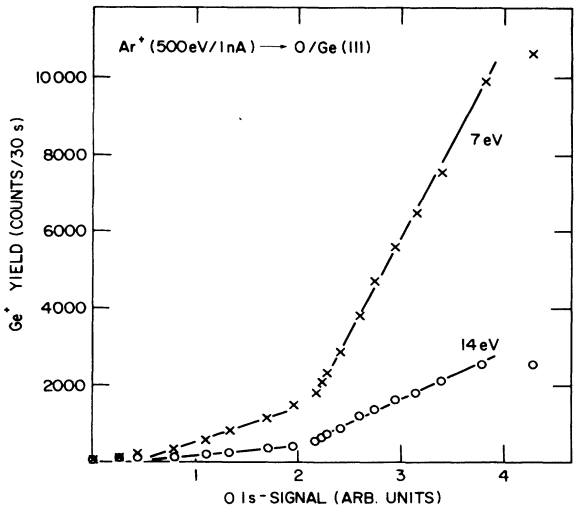

FIG. 5. Sputtered Ge^+ yield from oxygenated Ge surface at different oxygen coverages. The maximum coverage was about two monolayers.

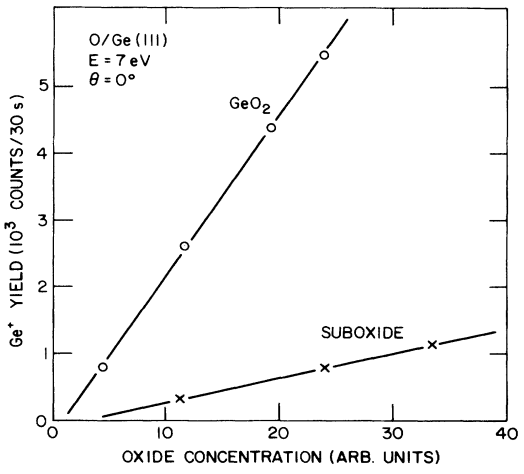

FIG. 6. Dependence of the sputtered Si^+ yield on the concentration of germanium suboxide and dioxide formed.

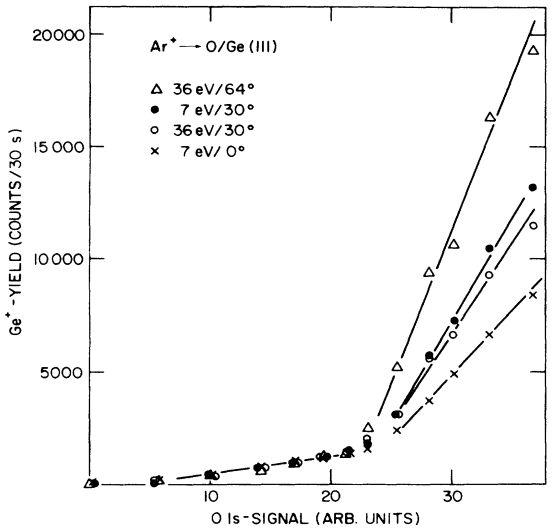

FIG. 7. Comparison of the oxygen coverage dependence of the Ge^+ yield at different emission angles and velocities. All the data have been normalized to the 7 eV/0° result at 22 units of O 1s signal.

were chosen to provide for the same value of $v_z(=4.3\times10^5$ cm/s) of the detected Ge^+ ions. The strong angular dependence contrasts the negative result observed for O-Si(100) although in both cases LEED data suggested the loss of long-range order upon oxidation. The data, however, implies a dependence of the secondary-ion emission process on the short-range order or the molecular orientation. Unfortunately, with the beam-detector geometry fixed, our apparatus was not adequate to perform a more detailed study of this interesting phenomenon.

The next most abundant secondary ion observed is O^- and is approximately one-sixth of the Si^+ yield. Unlike the O-Si(100) case, after increasing linearly with the suboxide concentration, the O^- yield stayed constant during the growth of GeO_2. All the observed molecular ion yields showed linear dependences with oxygen coverages in the two oxygen coverage regions with different slopes. While the GeO^+, GeO_3^- yields increased with the growth of GeO_2, the Ge_2O^+ and GeO_2^- yields actually decreased. Only Ge^+ and GeO^+ showed large emission angle dependences. We do not have a clear explanation of these behaviors at present although they all reflected the changes in the oxygen-germanium bonding configurations.

The following summarizes our experimental observations.

(a) In all the three chemical systems studied, N-Si(100), O-Si(100), and O-Ge(111), the reaction with the electronegative atoms nitrogen and oxygen enhances the emission of Si^+ or Ge^+ over the intrinsic ion yields from clean surfaces. The enhanced ion yields were linearly related to the amounts of compounds formed in accordance with Eq. (1).

(b) The Si^+ or Ge^+ yield goes up with the oxygen coordination of Si or Ge in the oxides formed, reflecting the sensitivity to the chemical environment.

(c) The sensitivity to the chemical environment decreases with increase in the emission velocity.

(d) No simple correlation with the normal component of the emission velocity v_z was observed. The strong angular dependence observed in O-Ge(111) may be the result of short-range order or molecular orientation. No angular dependence was observed in the O-Si(100) system.

IV. DISCUSSIONS

We have shown that Eq. (1) is a valid description of the Si^+ and Ge^+ secondary ion yields for all the three systems. The data are consistent with a local interaction for the ionization process. Here we would like to discuss two interesting observations that are frequently overlooked in SIMS experiments.

The concept of a site-dependent local sputtering coefficient Y_i was also introduced in the context of SIMS by Sigmund[21] in an integral form. As shown in our experiment, the secondary ion yield is proportional to the sum of the products $P_i^+Y_i$, but the separate determinations of P_i^+ and Y_i are very difficult. In conventional experiments, only the weight average $\tilde{Y}$ [Eq. (2)] is being measured. One possible way to determine Y_i is to perform a static mode sputtering experiment on single phase surfaces, e.g., SiO_2, so that no other phase is formed by the ion bombardment. Then Y_i can be determined if the total sputtered flux is measured, for example, by multiphoton ionization.[22]

The simple linear relations between I_M^+ and c_0, the concentration of the electronegative species, appear only in special cases. We observed them because special procedures were followed so that the individual phases of the reaction were well separated. Since the product $P_i^+Y_i$ is strongly site dependent, the secondary ion yield depends critically on the distribution of the f_i's. In conventional SIMS experiments with dynamic mode sputtering, ion-beam-induced mixing can compete with chemical kinetics. Oechsner and Sroubek[23] have modelled the case where the oxygen atoms are randomly distributed. In this special case, the distribution of the f_i's can be predicted and sites with higher oxygen coordination are favored at high oxygen concentrations. The ion yield has a power-law-like dependence on c_0. In practice, the distribution of f_i's can span between the random case to the case where the chemical kinetics dominates, depending on the experimental conditions. We have chosen the latter in our set of experiments. This also explains the divergence of the reported data on the oxygen concentration dependence of Si^+ yield sputtered from oxygenated silicon, as mentioned in the Introduction. Hence unless special attention is taken, the measured ionized probability $\tilde{P}^+$ will be a weighted average given by:

$$\tilde{P}^+=\sum_i f_i P_i^+ Y_i / \sum_i f_i Y_i \ . \tag{6}$$

In a recent paper,[6] we have proposed a semiquantitative bond-breaking model to explain the ionization of sput-

tered atoms. According to this model, the sputtering of an atom M from the surface leaves a cation vacancy X which can trap an electron for at least the sputtering time. Charge exchange can happen at the crossing between the diabatic covalent potential curve M^0+X^0 and the diabatic ionic curve M^++X^- at distance R_c from the surface. The crossing distance $R_c=(I-A)^{-1}$ in atomic units is the place where the electrostatic attraction in the ionic case balances the difference $I-A$. Here I is the ionization potential of M, and A is the electron affinity of X. The ionization probability P^+ is given by:

$$P^+\simeq G\exp(-2\pi H^2/v\mid a\mid)_{R=R_c}\ . \tag{7}$$

Here H is the transition matrix element, v is the velocity, and $\mid a\mid$ is the difference in the first derivatives of the potential curves, all evaluated at R_c in atomic units. G accounts for the degeneracies g_0 and g_+ of the covalent and ionic curves respectively, and equals approximately to g_+/g_0.

The matrix element H reflects the properties of the original chemical bond before M is sputtered. The yield ratio Y_R between the dioxides and suboxides measured is hence a measure of the change in H with the change in the chemical state. For simplicity, Eq. (7) can be written as $P^+/G=\exp[-\tilde{v}/v(R_c)]$ where $\tilde{v}(=2\pi H^2/\mid a\mid)$ absorbs all the variables in the exponent except $v(R_c)$. We shall first discuss the O-Si(100) case where there is no angular dependence.

By writing $\tilde{v}=v_1,v_2$ for the suboxide and dioxide phases respectively, the yield ratio is given by

$$Y_R=(Y_2G_2/Y_1G_1)\exp[(v_1-v_2)/v(R_c)]\ . \tag{8}$$

For a sputtered ion M^+ with mass m and emission energy E_k,$v(R_c)$ can be calculated:

$$v(R_c)=[2(E_k+I-A)/m]^{1/2}\ . \tag{9}$$

Figure 8 shows a semilog plot of the measured value of Y_R (Sec. III B) as a function of $[v(R_c)]^{-1}$ for Si^+. Indeed the data points follow a linear relation with $v_1-v_2=1.1\times10^6$ cm/s and $Y_2G_2/Y_1G_1=1.1$. This result is consistent with the bond-breaking model. If the degeneracies originate only from the sputtered M^0 or M^+,$G_1=G_2$ is a reasonable approximation. Then we obtain a rough estimate of the ratio of sputtering coefficients $Y_2/Y_1\simeq1.1$.

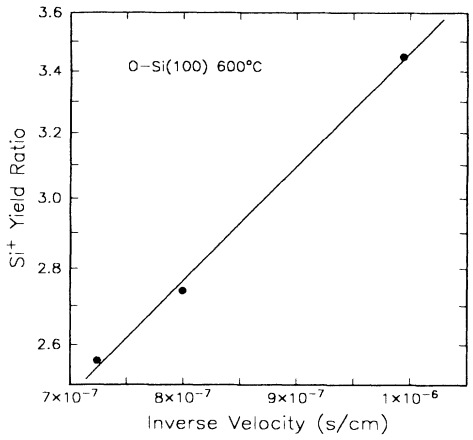

FIG. 8. The Si^+ yield ratio Y_R between silicon dioxide and silicon suboxide as a function of inverse of the Si^+ velocity at the crossing point.

We have observed large angular anisotropy in the value of Y_R for the O-Ge (111) system. There are two possible contributions to this effect. One is the angular anisotropy of the sputtering coefficients Y_1,Y_2 which relates to the anistropy of the momentum transfer in a crystalline lattice. The other possibility is related to the electron transfer. The transition matrix element H can be angular anisotropic. A possible way to separate these two contributions is to compare the angular distributions of the sputtered ions and neutral atoms. The recent progress in laser ionization[24] seems to offer this possibility.

We have, in this paper, reported experimental evidence that supports the local bond-breaking model. This, in combination with the electron tunneling model, can form a good basis for the further understanding of the nonadiabatic charge transfer phenomena between sputtered atoms and surfaces.

ACKNOWLEDGMENT

The authors would like to acknowledge useful discussions with J. Clabes, R. Kelly, N. D. Lang, S. Pantelides, W. Reuter, and K. Wittmaack.

[1]H. W. Werner, in *Electron and Ion Spectroscopy of Solids*, edited by L. Fiermans, J. Vennik, and W. Dekeyser (Plenum, New York, 1977).
[2]M. L. Yu and N. D. Lang, Nucl. Instrum. Methods B **14**, 403 (1986).
[3]M. L. Yu and N. D. Lang, Phys. Rev. Lett. **50**, 127 (1983).
[4]M. L. Yu, Phys. Rev. Lett. **47**, 1325 (1981).
[5]N. D. Lang, Phys. Rev. B **27**, 2019 (1983).
[6]M. L. Yu and K. Mann, Phys. Rev. Lett. **57**, 1476 (1986).
[7]G. Slodzian and J. F. Hennequin, C. R. Acad. Sci. Paris **263**, 1246 (1966).
[8]A. Benninghoven, Surf. Sci. **53**, 596 (1975).
[9]P. Sanda, U. Kaiser, R. Jede, D. Lipinsky, O. Ganchow, and A. Benninghoven, J. Vac. Sci. Technol. A **3**, 1946 (1985).
[10]K. Wittmaack, Surf. Sci. **112**, 168 (1981).
[11]V. R. Deline, W. Katz, C. A. Evans, Jr., and P. Williams, Appl. Phys. Lett. **33**, 832 (1978).
[12]H. Gnaser, Nucl. Instrum. and Methods **218**, 312 (1983).
[13]A. E. Morgan, H. A. M. de Grefte, N. Warmoltz, H. W. Werner, and H. J. Tolle, Appl. Surf. Sci. **7**, 372 (1981).
[14]A modified Bessel box from Extranuclear Laboratories Inc. was used. A grounded plate with fine wire mesh on the entrance hole was used to prevent extraction of secondary ions by the field of the energy analyzer. Occasionally, a voltage in

the order of 1 V was used to overcome the work function difference between the sample and the energy analyzer.

[15]A. G. Schrott, Q. X. Su, and S. C. Fain, Jr., Surf. Sci. **123**, 223 (1982).

[16]C. Maillot, H. Ronlet, and G. Defour, J. Vac. Sci. Technol. B **2**, 316 (1984). They reported a chemical shift of 2.7 eV. The discrepancy with our data may be a result of different crystallinity of Si_3N_4 formed under different growth conditions.

[17]W. H. Strehlow and E. L. Cook, J. Phys. Chem. Ref. Data **2**, 163 (1973).

[18]M. L. Yu, J. Clabes, and D. J. Vitkavage, J. Vac. Sci. Technol. A **3**, 1316 (1985).

[19]G. Hollinger and F. J. Himpsel, J. Vac. Sci. Technol. A **1**, 640 (1983).

[20]C. M. Garner, I. Lindau, J. N. Miller, P. Pianetta, and W. E. Spicer, J. Vac. Sci. Technol. **14**, 372 (1977).

[21]P. Sigmund in *Proceedings of SIMS IV,* Vol. 36 of *Springer Series in Chemical Physics,* edited by A. Benninghoven, J. Okana, R. Shimizu, and H. W. Werner (Springer-Verlag, New York, 1984), p. 2.

[22]F. M. Kimock, J. P. Baxter, D. L. Pappas, P. H. Kobrin, and N. Winograd, Anal. Chem. **56**, 2782 (1984).

[23]H. Oechsner and Z. Sroubek, Surf. Sci. **127**, 10 (1983).

[24]J. P. Baxter, G. A. Schick, J. Singh, P. H. Kobrin, and N. Winograd, J. Vac. Sci. Technol. A **4**, 1218 (1986).